Evolution of the optically detected magnetic resonance spectra of divacancies in 4*H*-SiC from liquid-helium to room temperature

Danial Shafizadeh, Nguyen T. Son, Igor A. Abrikosov, and Ivan G. Ivanov*
Department of Physics, Chemistry and Biology, Linköping University, SE-58183, Linköping, Sweden

(Received 29 December 2024; accepted 25 March 2025; published 2 April 2025)

The divacancies in 4*H*-SiC attract significant attention for use as qubits owing to their spin and photoluminescence (PL) properties and near telecom PL emission. Nevertheless, there exist some ambiguities in the interpretation of their optically detected magnetic resonance (ODMR) spectra, especially at elevated temperatures. In this study, we investigate the divacancy configurations PL1–PL7 using PL and ODMR. We record the full temperature dependence between liquid-helium temperature (3.8 K) and room temperature (295 K), obtained with two different laser energies and different laser polarizations. We also present PL data recorded simultaneously with the ODMR. Our study allows us to continuously follow the evolution of all divacancy configurations in ODMR with temperature, even though their signature is not distinguishable in PL at elevated temperatures. We identify all lines in the room-temperature ODMR spectrum and show that a hypothetical defect PL7, assumed in earlier work to stem from another divacancy configuration, does not exist and its ODMR signal at room temperature is fully explained with PL4. We also provide direct PL evidence on the spatial distribution of PL5, PL6, and a new PL3a defect, showing their presence only close to the surface of the sample, thus corroborating their association with divacancies near stacking faults. We address also the role of the upconversion of the photoluminescence in the ODMR spectra observed at higher temperatures.

DOI: 10.1103/PhysRevB.111.165201

I. INTRODUCTION

Spin-active photoluminescence (PL) defects in solids have attracted increasing attention due to their potential applications in quantum sensing, quantum communication, and quantum computing, with the NV center in diamond emerging as the leading contender [1–5]. Among these materials, silicon carbide (SiC) has recently emerged as a promising platform, which hosts various PL centers that emit light near and at telecom wavelengths suitable for applications in long-distance quantum communication using existing fiber networks [6,7]. Sharing the advantage of color centers in wide-band-gap semiconductors like diamond, defects in SiC also have long spin coherence times that can be optically controlled even at room temperature [7–10]. Additionally, SiC is a well-developed material with established large-scale manufacturing processes of high-purity wafers and mature nanofabrication techniques [11].

The neutral divacancy ($V_C\,V_{Si}^0$), i.e., an uncharged complex consisting of a C vacancy (V_C) and a nearest Si vacancy (V_{Si}), is one of the most studied defects in SiC. It has been identified by electron paramagnetic resonance (EPR) [12]. The PL signature related to this defect was later identified by PL and optically detected magnetic resonance (ODMR) measurements [8]. In the 4*H*-SiC polytype, there are two inequivalent lattice sites, a quasicubic (*k*) and a hexagonal (*h*) site, the local environment structure of which differs in the third-nearest neighbors. This leads to four distinguished divacancy configurations with two axial centers with both vacancies along the *c* axis at the *h* site PL1 (*hh*) and at the *k* site PL2 (*kk*), and two basal centers PL3 (*kh*) and PL4 (*hk*) [8]. In addition, the so-called divacancylike or "modified divacancy" PL5, PL6, and PL7 centers have been reported [8,13]. For PL5 and PL6 centers, their PL band and zero-phonon line (ZPL) have been identified [8] and the correlation with EPR has been made with both centers being slightly deviated from the axial symmetry [14]. However, the PL of the PL7 center has never been observed.

The previous temperature dependence study of ODMR of divacancies shows the observation of the PL7 signal at room temperature [13]. Although only one line was observed in the zero-field ODMR spectrum, PL7 was assigned to a basal divacancy [13]. [For a basal divacancy, with the presence of the fine-structure parameters D and E representing the zero-field splitting caused by the axial and orthorhombic field, respectively, two ODMR lines should be expected at frequencies $(D+E)$ and $(D-E)$ in ODMR measurements.] So far, the zero-field ODMR line at 1.333 GHz measured at room temperature [13] has become the signature of the PL7 center also in experiments performed at room and higher-than-room temperatures [15].

The PL5, PL6, and PL7 centers have been suggested to be divacancies positioned in the vicinity of a stacking fault

*Contact auhtor: ivaiv28@liu.se

[16]. The stacking fault acts as a local quantum well within the 4*H*-SiC lattice, which helps to stabilize the charge state of these point defects. In addition to having stable and bright emissions, modified divacancies show higher-readout ODMR contrasts (∼20%–30% for PL5 and PL6) compared to those of conventional divacancies PL1 – PL4 (typically 3%–7%) [15]. These features make the modified divacancies more favorable than conventional divacancies for applications in quantum technologies.

Realization of modified divacancies requires ion implantation, which creates both stacking faults and vacancies. It is therefore expected that the density of modified divacancies is less than that of conventional divacancies in a SiC layer implanted with low ion fluences for single defect studies. However, recent experiments on C^+ ion implantation show that in a 10 × 10 array of implanted sites, one single emitter PL6 and seven single emitters PL7 were observed [15]. It is noticed that PL6 is confirmed by both PL and ODMR, while PL7 is assigned based only on the ODMR signal at 1.333 GHz [15]. The reliability of such assignment for PL7 may be questionable, considering that all the PL1–PL7 centers give rise to ODMR signals in the narrow frequency range of $1.305 - 1.365$ GHz [13], making it difficult to distinguish between them.

In this study, PL and ODMR are used to study the properties of the divacancies. We found that all divacancy centers in 4*H*-SiC can be excited by laser with photon energies lower than the energy of the ZPL, i.e., anti-Stokes excitation. The phonon-assisted mechanism is found to be responsible for the observed upconversion process, which becomes more efficient at elevated temperatures. By combining Stokes and anti-Stokes excitation with different laser polarizations in the temperature dependence studies of PL and ODMR of divacancies, signals from different divacancy configurations can be followed from ∼4 K to room temperature. This allows conclusive confirmation that (i) the positive ODMR peaks of PL3 and PL4 disappear at elevated temperatures, and thus, only their negative peaks remain at room temperature, and (ii) the PL7 center does not exist and the ODMR signal previously assigned to PL7 is the high-frequency line of PL4. The disappearance of the positive, low-frequency ODMR peak of PL4 at elevated temperatures leads to the incorrect conclusion that PL4 is not detected at room temperature and, consequently, its negative peak, which survives at room temperature, has wrongly been assigned to a new PL7 center [13]. The disappearance at higher temperatures of all positive ODMR peaks, the high-frequency peak of PL3, the low-frequency peak of PL4, and the only (positive) peak of PL2, is also observed. This phenomenon is not understood at present but is probably due to peculiarities of the spin-selective transitions from the ^3E excited state to the $^3A_2$ ground state of the basal divacancies PL3 and PL4 with low symmetry C_{1h}. The observation possibly indicates also that the fine-structure parameters E of PL3 and PL4 have different signs.

The remainder of the article is organized as follows. Section II provides details on the samples, PL and ODMR setups, and experimental procedures. In Secs. III and IV, we present and discuss the results on the temperature dependence of PL and ODMR of divacancies under Stokes and anti-Stokes excitation with various laser polarizations. We address the incorrect assignment of the PL4 signal to a new center PL7. Finally, Sec. V provides a summary of the results.

II. EXPERIMENTAL

The sample containing divacancies is from a commercial as-grown bulk, high-purity semi-insulating (HPSI) 4*H*-SiC wafer, without any postgrowth processing apart from polishing. The low- and room-temperature PL spectra of the sample exhibit dominating emission from divacancy-related defects (PL1 – PL6) with weak contribution from the vanadium-related lines (∼1278 nm), as illustrated later. One important property of this sample is the absence of quenching in the divacancy PL at low temperature for all excitation photon energies used in this scope. We recall that the low-temperature PL (LTPL) of the divacancies in common samples (HPSI or n-type) quenches when the excitation photon energy is below ∼1.3 eV (wavelength > ∼970 nm), with slightly different thresholds for PL1 – PL4 [17–19]. In the case of quenching, a repump laser at higher energy is needed to maintain steady PL intensity. However, a repump laser would also serve as an excitation source, thus interfering with the selective excitation experiments presented previously [20] and discussed here. Hence, the stability of the PL with excitation energies below ∼1.3 eV is a condition for most of the results presented here and is fulfilled by the sample used in this study. The reason for stable PL in this sample is the absence of filled electron traps in the upper half of the band gap, which might be photoionized by the laser excitation and cause PL quenching [17]. This notion is corroborated by the observation of the electron-spin-resonance spectrum of the positively charged carbon vacancy (V_C^+) in this sample [17], suggesting that the Fermi level is at or below that of V_C^+ (∼1.8 eV below the conduction band) [21].

The PL measurements were carried out using a Jobin Yvon HR460 monochromator equipped with a 300-g/mm grating and InGaAs multichannel detector. Tunable Ti-sapphire and diode-based Toptica lasers were used for variable excitation of the divacancy defects. The sample was mounted in a variable-temperature closed-cycle cryostat that can be cooled to 3.8 K. The resolution of ∼4 Å with the 300-g/mm grating and 50-μm monochromator slit is sufficient for the low-temperature measurements. A halfwave plate was placed in the path of the laser for rotating the laser polarization. The laser line is filtered using a variety of long-pass and band-pass filters from Thorlabs. For the ODMR measurements, a 50-μm-thick copper wire was used as a microwave antenna oriented perpendicular to the c axis [details on the experimental geometry are provided in Fig. S1 and Sec. 1 of the Supplemental Material (SM) [22], see also the inset in Fig. 6(a)]. A superconducting nanowire detector from Quantum Opus coupled to an event timer and TCSPC module (HydraHarp 400 from PicoQuant) were used for detecting the integrated PL signal from divacancies in the ODMR measurements.

III. RESULTS

A. General consideration

In a recent work [20], we described selective excitation of only one of the four configurations of the divacancy, namely,

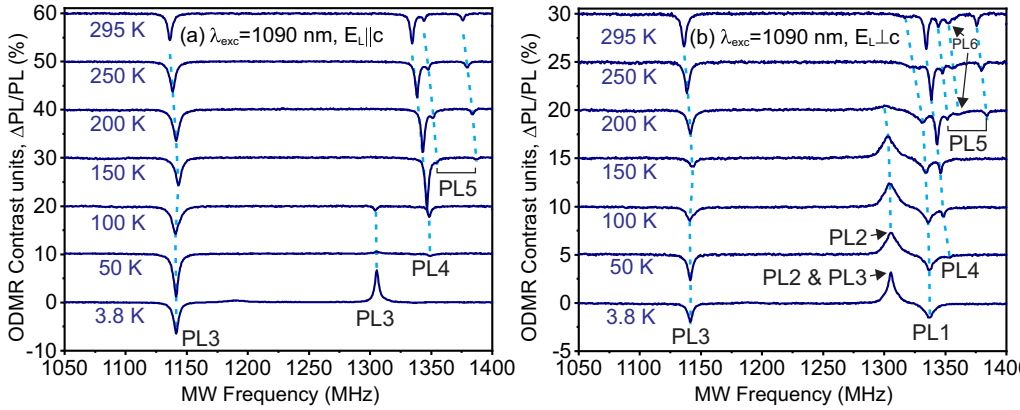

FIG. 1. Temperature dependence of continuous wave (CW) ODMR of divacancies in 4*H*-SiC obtained with excitation wavelength of 1090 nm. Excitation polarization in panel (a) is parallel to the *c* axis ($E_L||c$), and in (b) perpendicular to the *c* axis ($E_L \perp c$). The vertical units are common for all spectra (ΔPL/PL in percent), but the spectra are shifted vertically by 10 (5) percent units for the left (right) panel for better visibility.

the *kh* configuration for $V_C V_{Si}$, with the corresponding PL3 ZPL. The corresponding ODMR spectrum contains a contribution from this configuration, and it is interesting to see if this selective excitation can be implemented also at higher temperatures. This motivated a study of the temperature dependence of the ODMR and PL spectra presented in this work. To understand the structure of the ODMR spectrum at elevated temperatures, we use two different excitations with different polarizations, parallel (E||c) and perpendicular (E⊥c) to the crystal *c* axis. The one excitation is at 1090 nm (1.137 eV), which is in the anti-Stokes region (at lower energy) of the PL4 ZPL (1078 nm, 1.149 eV) but in the Stokes region of PL3 (1107 nm, 1.119 eV), and is hence capable of exciting the latter. When this excitation is used with E||c polarization at liquid-He temperature, selective excitation of PL3 is implemented, because the PL1 and PL2 configurations cannot be excited with E||c [20], even though these ZPLs have lower energies than PL3. However, when the temperature increases new lines appear in the ODMR spectrum and, using experimental data obtained with a second excitation at 940 nm, we can identify the origin of these new lines. The latter excitation has energy of 1.319 eV, which is higher than the ZPL energies of all divacancy configurations PL1 – PL6 (1.095 – 1.194 eV). Eventually, the origin of all lines constituting the room-temperature ODMR spectrum is established, and we show that the alleged PL7 defect associated with a room-temperature line at 1.333 GHz [13,15] is in fact the contribution from the PL4 configuration.

Some experimental evidence that the selection rule stated above is valid also for room temperature is presented in Fig. S2 and Sec. 2 of the SM [22].

B. Laser excitation in the anti-Stokes region of PL4 (1090 nm, 1.137 eV)

When this excitation is applied with E||c polarization, no contribution in the PL or the ODMR is expected from the axial configurations PL1 and PL2 [20]. In addition, when the temperature is in the range of liquid-He temperature, there will be no contribution from PL4 either because the excitation at 1.137 eV has lower energy than the PL4 ZPL (1.149 eV). The only contribution observed in ODMR and PL is from PL3, as illustrated by the lowermost curves in Figs. 1(a) and 2(a) for the ODMR and the PL spectrum, respectively.

Using polarization E⊥c brings up the contribution of the axial configurations PL1 and PL2, but PL4 remains inactive at low temperature [cf. the lowermost curves in Figs. 1(b) and 2(b) for ODMR and PL, respectively]. We notice that, unlike the basal configurations with lower symmetry (C_{1h}), the axial configurations with C_{3v} symmetry exhibit a single ODMR line, negative for PL1 and positive for PL2. We notice also that the positive PL2 ODMR line coincides almost exactly with the positive peak of the PL3 line [8], which can also be seen in our low-temperature spectrum [lowermost curve in Fig. 1(b)]. At 50 K and higher temperatures, the positive peak in ODMR of PL3 vanishes [nearly undetectable already at 50 K, see Fig. 1(a)], while the PL2 peak persists up to ∼150 K, then rapidly decreases and vanishes completely at room temperature.

The PL spectra measured for each temperature and laser polarization at the same time as the ODMR spectra are displayed in Fig. 2. At low temperatures the ZPLs are well distinguishable, and it can be seen from Fig. 2(a) that the PL1 and PL2 lines vanish for E||c laser polarization but appear in the low-temperature spectra recorded with E⊥c, as expected [20]. However, the appearance of several other peaks in the ODMR spectra at elevated temperatures apart from those associated with PL1, PL2, and PL3 requires further understanding. We notice that at elevated temperatures the high-energy part of the PL spectrum rises and is likely to extend below the long-pass filter cutoff at 1100 nm (the cutoff is clearly seen in all spectra above ∼150 K in Fig. 2). This observation suggests that there exists significant upconversion in the spectra at higher temperature, i.e., the divacancy configurations with ZPLs above the laser energy also are excited and observed in ODMR. This notion was confirmed in two subsequent experiments described in the following sections. In the first experiment we use an excitation wavelength (940 nm, 1.319 eV) with photon energy higher than that of all divacancy ZPLs, including PL5 and PL6 (the latter appear at 1.190 and 1.194 eV, respectively).

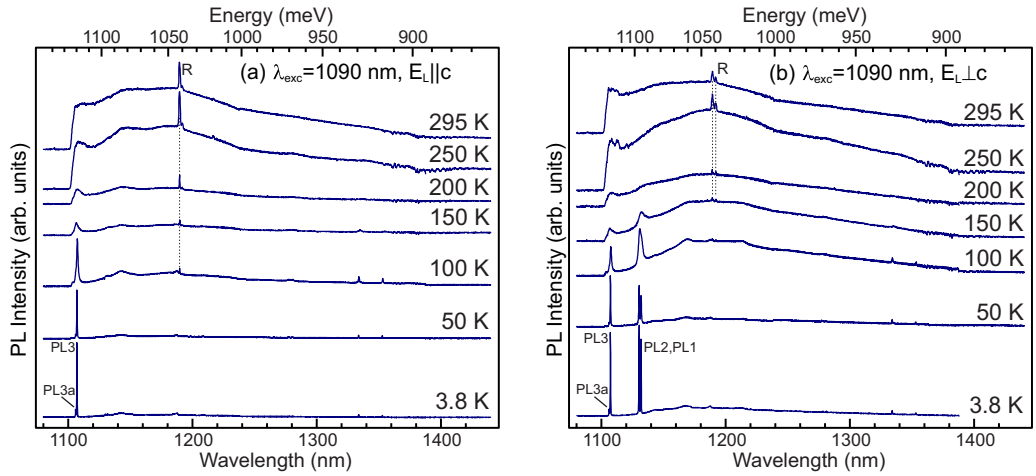

FIG. 2. PL spectra obtained at the same time as the ODMR spectra in Fig. 1: (a) $E_L||c$ and (b) $E_L \perp c$. Different scaling factors are applied to the different spectra for better visibility. Notice the increase of the intensity of the broadband emission towards shorter wavelengths (higher energies) with increasing temperature, a consequence of the upconversion by phonon-assisted absorption. "R" denotes the Raman lines.

In the second experiment, we use a double monochromator for detection of the PL. In that case no filter is needed in the PL collection path, and detection of the spectrum at energies higher than the laser energy becomes possible. The results of these experiments are described in more detail below.

Another important observation from the PL spectra displayed in Fig. 2 is the appearance of the peak denoted PL3a here at 1106.2 nm, just 1 nm below the PL3 line. This peak, which is rather weak compared to PL3 when 1090-nm excitation is used, becomes much more prominent with the 940-nm excitation. This peak will be discussed further in Secs. III E and IV.

C. Laser excitation in the Stokes region of all divacancy configurations (940 nm, 1.319 eV)

With this excitation, all divacancy configurations (PL1–PL6) are excited and contribute to both the ODMR and PL spectra, as illustrated in Figs. 3 and 4. However, in agreement with the selection rules [20], excitation with E||c polarization cannot excite the axial configurations (PL1, PL2, and PL6), and hence their signatures are absent in the corresponding ODMR and PL spectra [Figs. 3(a) and 4(a), respectively]. As noted earlier, the PL3a line is also observed, and its intensity compared to that of the PL3 line is larger than in the case of 1090-nm excitation. The PL spectra in Fig. 4 also illustrate that no emissions from other defects apart from PL1–PL6 and PL3a are detected in this sample.

The main result from those obtained with this excitation ODMR spectra is that the same number of ODMR peaks at the same positions are observed as in the case of 1090-nm excitation in the room-temperature spectra, if the individual spectra obtained with the same laser polarization are compared [cf. the topmost curves in Figs. 1(a) and 3(a), and Fig. 1(b) and 3(b) for E||c and E⊥c polarizations, respectively]. Furthermore, using the temperature dependence of the ODMR spectra, each of the peaks in the room-temperature ODMR spectra can be traced down to their position at the lowest temperature of 3.8 K, for both excitation polarizations. The contributions of the various divacancy configurations to the low-temperature ODMR spectrum are well known [8]; hence we can

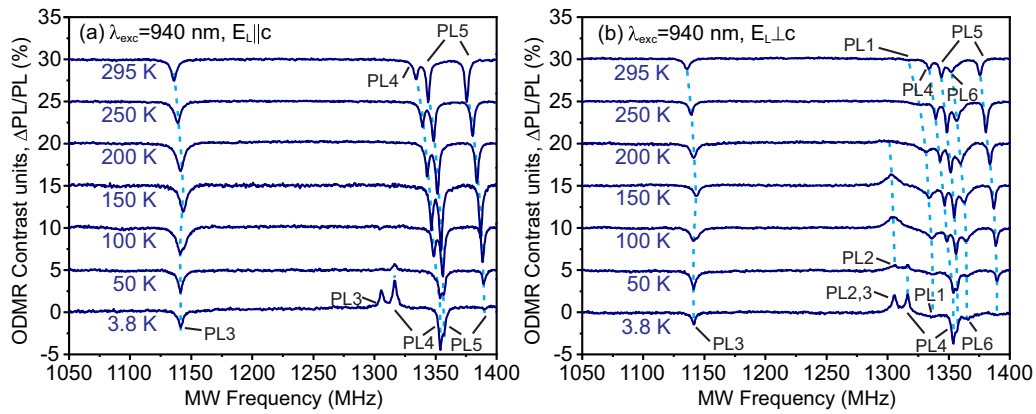

FIG. 3. Temperature dependence of the ODMR spectra obtained with 940-nm excitation with polarization (a) $E_L||c$ and (b) $E_L \perp c$. The vertical-axis units are the same as in Fig. 1, ODMR contrast percents. The spectra are shifted vertically by 5% for better visibility. Note that the positive peak of PL4 vanishes above ∼50 K, similar to the positive peak of PL3.

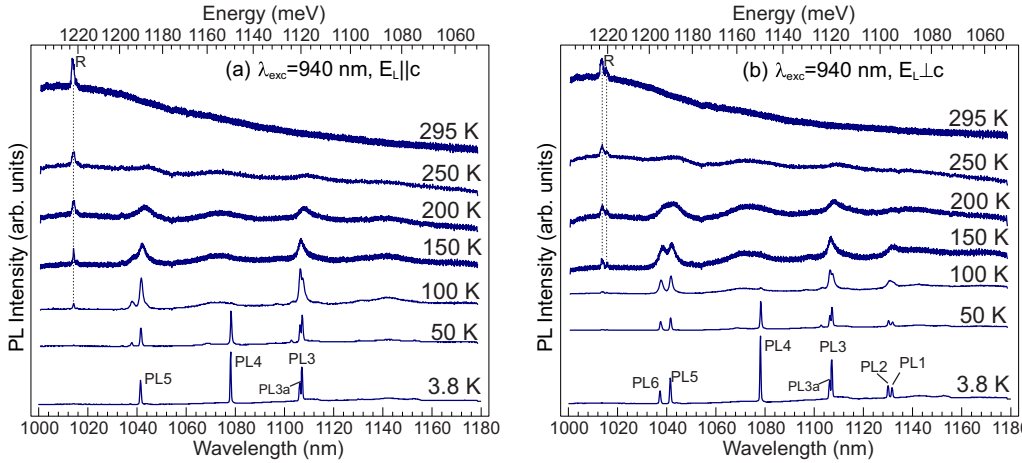

FIG. 4. Temperature dependence of the PL spectra obtained at the same conditions as the corresponding ODMR spectra in Fig. 3 [940-nm excitation with polarization (a) $E_L||c$ and (b) $E_L \perp c$]. The spectra are rescaled with different factors and shifted vertically for viewing convenience. "R" denotes the Raman lines.

identify also the origin of all peaks in the room-temperature spectrum.

We now discuss the existence of the defect termed PL7 in previous work [13,15,23]. This defect is associated with a peak at 1333 MHz in the *room-temperature* ODMR spectrum, but its low-temperature signature in PL has never been identified. In these previous works only the ODMR spectra above room temperature have been claimed to display a contribution from the alleged PL7 defect, whereas the full temperature dependence between liquid-helium and room temperature presented here in Figs. 1–4 clearly indicates that the peak at 1333 MHz is actually related to the PL4 line (see the eye-guiding lines in these figures). Moreover, the positive (low-frequency) peak of PL4 disappears already at ∼50 K (see Fig. 3), which is why only the contribution from the high-frequency peak remains at higher temperatures. This can be misinterpreted as an appearance of a new defect (i.e., PL7) with a single ODMR line. Hence, our data shows that the PL7 defect proposed in earlier work and associated with this peak is not a new defect but stems from PL4.

The ODMR peak positions at liquid-helium temperature (3.8 K) and at room temperature (295 K) are summarized in Table I, and the temperature dependence of all ODMR peak positions is displayed in Fig. 5. We notice that the PL4 ODMR peak position at 295 K appears between 1333 and 1334 MHz in our measurement but closer to 1334 MHz, hence the value 1334 MHz in Table I. According to Fig. 5, the PL4 negative ODMR peak exhibits a strong temperature dependence, especially towards room temperature (estimated 0.12 MHz/K), which may affect the exact peak position in view of some arbitrariness in defining the room temperature (e.g., 300 K in [23] and 295 K in this work).

D. The impact of the PL upconversion on the ODMR spectra at higher temperatures

As already mentioned in Sec. III B, the appearance of new lines in the ODMR spectra obtained at higher temperatures can be understood in terms of upconversion of the luminescence from centers, for which the excitation is in the anti-Stokes region (at energy lower than the ZPL energy). Upconversion has been observed earlier for the silicon vacancy [17,24] and for one of the divacancy configurations, PL6 [25]. In both latter works [24,25] the upconversion is

TABLE I. Summary of the line positions, their configurations, and zero-field splitting obtained by ODMR for the divacancies and the modified divacancy configurations PL5 and PL6 in 4*H*-SiC at low (3.8 K) and room temperatures.

Line	f (MHz)[a]	f (MHz)[b]	Position in nm (meV)	Axial/basal	Identification
PL1	1336	1317	1132.0 (1095.0)	Axial	hh
PL2	1305.5	–	1130.5 (1096.5)	Axial	kk
PL3	1141.5	1136	1107.6 (1119.1)	Basal	kh
	1305.5	–			
PL4	1354	1334	1078.5 (1149.3)	Basal	hk
	1316.5	–			
PL5	1389.5	1375	1041.9 (1189.9)	Basal	–
	1356.5	1344			
PL6	1366	1352	1037.7 (1194.8)	Axial[c]	–

[a]Measured at 3.8 K.
[b]Measured at room temperature (295 K).
[c]According to Ref. [14], there is slight deviation from axial symmetry for PL6.

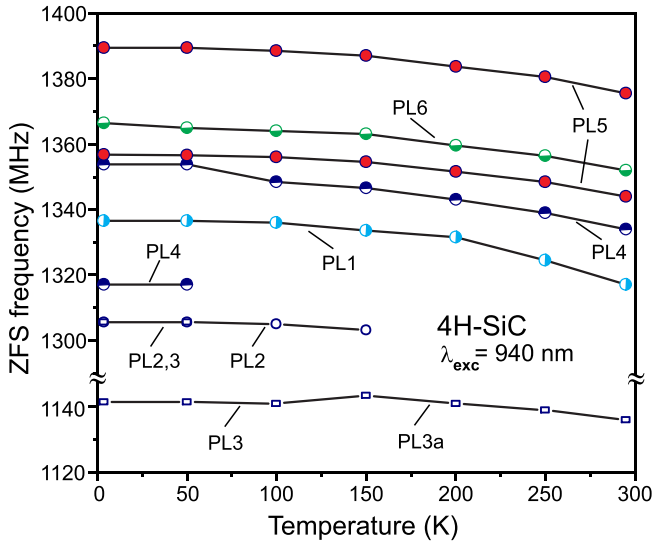

FIG. 5. Temperature dependence in the interval 3.8–295 K of all ODMR peaks for all divacancy configurations PL1–PL6 with laser excitation at 940 nm. The lines terminating at lower temperatures are associated with the positive peaks vanishing with rising temperature (PL4 low frequency, PL3 high frequency, and PL2). Notice the anomalous behavior of the PL3 low-frequency peak assumed to be due to two defects, PL3 (dominating below 100 K) and PL3a (dominating above 150 K).

explained in terms of phonon-assisted absorption. In this process, a phonon adds its energy to the insufficient-for-excitation energy of a laser photon (in the anti-Stokes region of the ZPL) to excite the center. The phonon needed for this process must exist; hence, upconversion excitation efficiency grows with the number of available phonons, i.e., with temperature, and is negligible at liquid-helium temperatures.

The notion of upconversion can be easily checked if the PL spectra are measured in the anti-Stokes region of the excitation, i.e., at shorter wavelengths than the laser wavelength. For this purpose, we utilize a double monochromator so that the use of a filter (either long pass or short pass) is not needed. While no upconversion can be seen at liquid-helium temperatures when 1089-nm (1.13-eV) excitation is used, at a temperature ∼80 K the ZPL PL4 is clearly observed. Therefore, the phonon sideband of PL4 extending well above 1100 nm (the cutoff wavelength of the long-pass filter used for the ODMR measurement) contributes to the ODMR lines observed for PL4 at elevated temperature. Their attribution to PL4 is corroborated by the ODMR spectra measured with 940-nm excitation, where the position variation of each line with temperature can be traced for the whole temperature range from 3.8 to 295 K, as already discussed in the previous section. Similarly, at higher temperatures the phonon-assisted upconversion with 1089-nm excitation leads to excitation of the PL5 and PL6 lines, and their contribution to the ODMR spectrum appears owing to their phonon sidebands extending beyond the cutoff of the long-pass filter (1100 nm). Efficient upconversion leading to excitation of PL5 and PL6 appears at higher temperatures than that for the PL4 line, because PL5 and PL6 are further away from the laser line, which requires higher-energy phonons for upconversion. For comparison, when 1089-nm (1.137-eV) laser excitation is used, the distance between the energy positions of the laser line and the PL4 ZPL is only ∼12 meV, while the distances to the PL5 and PL6 lines are about 53 and 57 meV, respectively. Thus, the excitation of PL5 and PL6 by upconversion requires higher temperature than that for PL4, as observed experimentally (see Fig. 1). Another consequence of the higher temperatures needed for observation of PL5 and PL6 in ODMR with 1089-nm excitation is that at these temperatures the ZPLs of these two defects are not well distinguishable anymore in the anti-Stokes region of the spectrum. However, the phonon sidebands appear and become well pronounced already at about 200 K, as seen from the short-wavelength band rising with temperature in the spectra of Fig. 2. Further experimental data, including direct observation of the ZPLs in the anti-Stokes region of the laser, is presented in the SM file [22] (Fig. S4).

Another experiment agreeing with the concept of phonon-assisted upconversion is presented in the SM file [22] (Fig. S3). In this experiment the ODMR spectra are measured at the same room temperature but using different laser wavelengths in the anti-Stokes region for PL5 and PL6. As the laser energy decreases, the efficiency of upconversion processes exciting PL5 and PL6 decreases, since the temperature and, therefore, the available phonon bath is kept constant, but the energy distance between PL5, PL6, and the laser line increases, demanding higher-energy phonons for upconversion.

E. Spatial distribution of the divacancy defects

Due to our experimental geometry and the polarization properties of the divacancy defects, all our PL and ODMR spectra are measured with the emission collected from the edge of the sample but very close (within 10–20 μm) to the surface of the chip, as illustrated in the inset in Fig. 6(a). This configuration is denoted as "Edge near surface" in Fig. 6. We notice that if the laser spot is moved towards the middle of the edge between the two surfaces of the specimen, the PL5, PL6, and PL3a lines vanish completely. This is illustrated in Fig. 6, with two series of spectra measured at different temperatures from the cleaved and polished edge of the sample in the middle of the edge [Fig. 6(b)], and from the edge but close to the surface, repeating the geometry used for the ODMR measurements [Fig. 6(a)]. Figure 7 zooms to the ZPL spectral range for PL1–PL6 in the temperature range 3.8–150 K, where the ZPLs are still distinguishable. Figure 6(a) clearly illustrates the peak shift of the broad emission at elevated temperatures from about 1180 nm (up to 200 K) to below 1120 nm at 250 K. This shift can be attributed to the dominant contribution of the PL5–PL6 emission in the spectrum above ∼200–250 K. Such a shift does not occur for the spectra measured in the middle of the edge far from the surfaces [Fig. 6(b)], indicating no contribution from PL5, PL6. The idea that PL5 and PL6 can only be observed near the surface of the sample is further corroborated by the detailed view in Fig. 7 in the temperature interval for which all zero-phonon lines are still distinguishable. The PL5 and PL6 ZPLs are only observed near the surface of the sample. This observation agrees with a previous report concerning the spatial distribution of PL6 only near the surface [16]. The current model for the origin

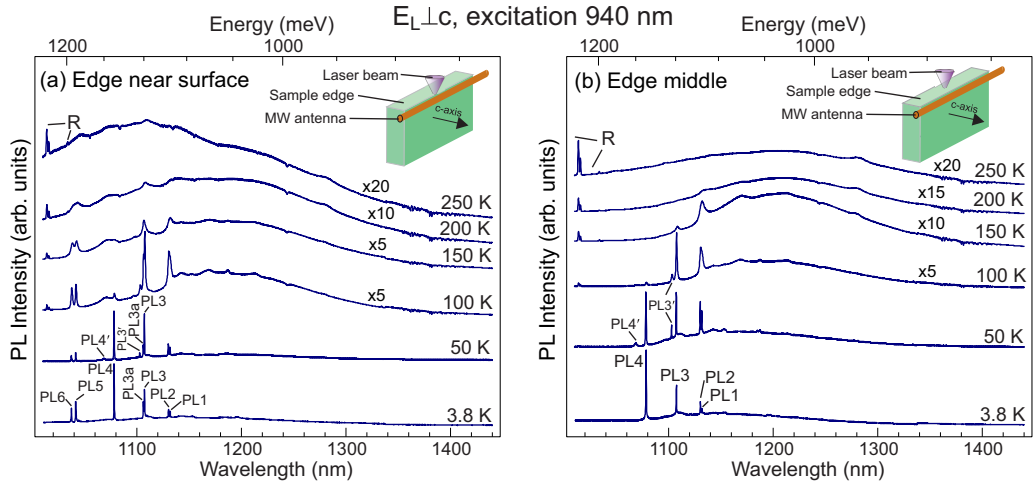

FIG. 6. PL spectra measured with excitation of 940 nm in the temperature interval 3.8–250 K from the edge of the sample but in two different positions on the edge: (a) close to the surface and the microwave (MW) antenna (a wire 50 μm in diameter) and (b) in the middle of the edge between the two faces of the sample. The inset illustrates the two experimental configurations; the rest of the measurements presented in this scope are conducted in configuration (a). Measurement from the edge of the sample is required for excitation with different laser polarizations ($E_L||c$ or $E_L \perp c$), and excitation close to the MW antenna is needed for effective coupling to the MW field. PL3′ and PL4′ stem from a second excited state associated with the splitting of the ^3E excited state in C_{1h} symmetry. "R" denotes the Raman lines.

of PL5 and PL6 is that of divacancies located near stacking faults, since an abundance of stacking faults due to polishing is anticipated near the sample surface. We need to mention here that the cleaved edge of the sample used in our study was also polished after cleaving to improve the PL signal from the edge of the sample. However, this polishing performed in a plane parallel to the crystal c axis may act differently in creating stacking faults compared to the usual polishing of a c-plane sample (perpendicular to the c axis). Our observation is that the edge polishing did not lead to an appearance of the PL5 and PL6 lines away from the c-plane surfaces of the sample.

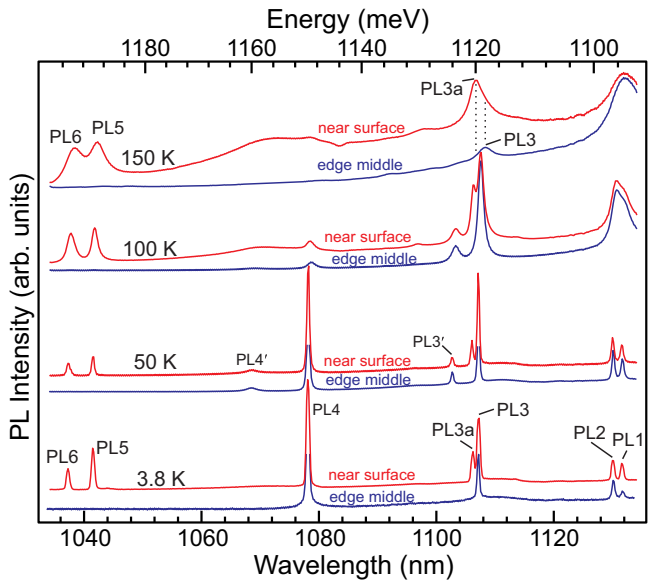

FIG. 7. High-resolution zoom into the short-wavelength part of the spectra presented in Fig. 6 for the temperature range 3.8–150 K, for which the ZPLs of the divacancy configurations are still distinguishable. The spectra marked "near surface" correspond to the spectra in Fig. 6(a) (the experimental geometry used throughout this work), and the rest marked "edge middle" are from Fig. 6(b). The figure clearly demonstrates the vanishing of the PL5, PL6, and PL3a defects away from the surface of the sample.

Furthermore, Fig. 7 illustrates that the PL3a line is also observed only near the surface and vanishes in the bulk of the sample. This is clearly seen in the spectra measured up to 100 K, where the ZPLs of PL3 and PL3a are still resolved. At 150 K, only the PL3 line is anticipated in the middle of the sample far from the surface. Close to the surface, the PL3a line dominates the emission in the ZPL region of PL3–PL3a, and the broad peaks corresponding to these two ZPLs are clearly shifted from each other (cf. the uppermost two spectra in Fig. 7).

We notice that owing to the small thickness of the sample (350 μm), we were unsuccessful in positioning the microwave antenna along the edge close to the middle and measure the ODMR spectra without the contribution from PL5, PL6, and PL3a.

IV. DISCUSSION

Figure 5 displays the temperature dependence of the ODMR peaks for the different divacancy configurations following the data obtained with 940-nm excitation, because in this case we observe the contribution from all configurations already at the lowest temperature of 3.8 K. One can notice two features in the ODMR spectra. First, we notice that all positive ODMR peaks observed at low temperature vanish completely at room temperature. This observation explains the statement in previous work that the PL2 ODMR line is not observed at room temperature [13,24,25], because PL2 only possesses a single positive ODMR peak. Thus, the ODMR spectra of all divacancy configurations at room temperature consist only of negative peaks (see Figs. 1 and 3).

Secondly, while the ODMR lines due to PL1, PL2, and PL4–PL6 exhibit redshift of their positions, as expected, because the lattice expansion with temperature is expected to diminish the spin-spin interaction responsible for the ground-state splitting observed in ODMR, the temperature dependence of the negative peak of PL3 exhibits unusual behavior, as seen in Fig. 5 where the temperature dependence of all ODMR peaks is summarized. (The positive peak of PL3 vanishes already above ∼50 K, see Fig. 1). At first the peak position slightly decreases; then at ∼150 K it jumps back to an even higher value than the low-temperature position, after which the redshift continues with increasing temperature, as expected. We notice also that in the range 4–295 K the redshift for this line is substantially smaller (∼5 MHz) than that for the other ODMR lines (∼15–20 MHz, see Fig. 5). This anomalous temperature behavior of the peak position is likely due to the influence of PL3a. We also observe the visibly broader and structured peak at 100 K, as if at this temperature two closely overlapping peaks contribute to the signal (see Figs. 1 and 3, the doublet structure is well visible for both laser polarizations at 100 K in Fig. 3).

We tentatively assign the anomalous temperature behavior of the PL3 peak to the overlapping contribution from two defects, as also witnessed from the visually double-peak appearance of the ODMR peak at 100 K (see, e.g., Fig. 3). Since at 100 K the contributions of PL3 and PL3a are quite similar (Fig. 7, Fig. 4), it is reasonable to assume that the second defect responsible for the second line in the ODMR peak of PL3 at 100 K is PL3a. If we further assume that at temperatures higher than 100 K the PL3a contribution is dominant (as seen from the PL spectra in Fig. 7, topmost two curves), then we can infer that the temperature dependence of the ODMR peak above 150 K simply reflects the behavior of PL3a, not of PL3. The latter dominates the ODMR signal in this region below ∼100 K, and the switching point between the dominant contribution from PL3 and from PL3a is around 100 K.

Finally, we suggest that PL3a originates from another divacancy configuration, possibly in the vicinity of stacking faults, which has not been explored so far. Since the excitation of PL3a is insensitive to the polarization of the exciting laser, it is plausible that this is another basal divacancy configuration, even though we identify only one of the anticipated two peaks for a basal configuration. This scenario is plausible if one assumes that at the temperature when PL3a dominates (above 100 K), the second ODMR peak, being positive, has already vanished, similar to the vanished positive high-frequency component of PL3.

V. SUMMARY

In this study we investigate the properties of divacancies in 4*H*-SiC using PL and ODMR techniques. Measurements of the temperature dependence of the ODMR and PL spectra in the range 3.8–295 K reveal that at elevated temperatures upconversion processes are activated and lead to excitation of divacancy configurations with ZPL emissions at higher energies than that of the laser line. This notion is confirmed by using two excitation laser energies, one at 1089 nm in the anti-Stokes region of PL4, PL5, and PL6, and one at 940 nm above the ZPL energies of all divacancy configurations. The orientation of the laser polarization with respect to the crystal *c* axis ($E_L||c$ or $E_L \perp c$) is used to switch the contribution of the axial divacancy configurations in the ODMR and the PL spectra off or on. We demonstrate that the selection rule stating that the axial configurations cannot be excited with $E_L||c$ polarization remains valid at all investigated temperatures. The experimental approach used here allows us to identify the origin of all ODMR lines at room temperature and shows that an ODMR peak at 1333 MHz previously associated with a presumably new PL7 defect is in fact due to the *hk* configuration PL4. An extra peak termed PL3a is observed near the surface of the sample and tentatively associated with a basal divacancy configuration modified by the nearby presence of a stacking fault. Finally, our observation that positive peaks of all divacancy configurations vanish at room temperature is not fully understood at present and requires further study.

ACKNOWLEDGMENTS

Financial support from the Knut and Alice Wallenberg Foundation (KAW 2018.0071) and the European projects under Horizon Europe (QRC-4-ESP, Project No. 101129663, and QUEST, Project No. 101156088) is acknowledged. D.S. acknowledges support from the AFM, Linköping University (CeNano grant 2021). N.T.S. acknowledges support from Vinnova (Grant No. 2024–00461). I.A.A. is grateful for the support by the Swedish Government Strategic Research Area in Materials Science on Functional Materials at Linköping University (Faculty Grant SFOMat-LiU No. 2009 00971).

DATA AVAILABILITY

The data that support the findings of this article are not publicly available upon publication because it is not technically feasible and/or the cost of preparing, depositing, and hosting the data would be prohibitive within the terms of this research project. The data are available from the authors upon reasonable request.

[1] M. H. Abobeih, J. Randall, C. E. Bradley, H. P. Bartling, M. A. Bakker, M. J. Degen, M. Markham, D. J. Twitchen, and T. H. Taminiau, Atomic-scale imaging of a 27-nuclear-spin cluster using a quantum sensor, Nature (London) **576**, 411 (2019).

[2] S. L. N. Hermans, M. Pompili, H. K. C. Beukers, S. Baier, J. Borregaard, and R. Hanson, Qubit teleportation between non-neighbouring nodes in a quantum network, Nature (London), **605**, 663 (2022).

[3] D. D. Awschalom, R. Hanson, J. Wrachtrup, and B. B. Zhou, Quantum technologies with optically interfaced solid-state spins, Nat. Photonics **12**, 516 (2018).

[4] M. Atatüre, D. Englund, N. Vamivakas, S.-Y. Lee, and J. Wrachtrup, Material platforms for spin-based photonic quantum technologies, Nat. Rev. Mater. **3**, 38 (2018).

[5] J. R. Weber, W. F. Koehl, J. B. Varley, A. Janotti, B. B. Buckley, C. G. Van de Walle, and D. D. Awschalom, Quantum

computing with defects, Proc. Natl. Acad. Sci. USA **107**, 8513 (2010).

[6] N. T. Son, C. P. Anderson, A. Bourassa, K. C. Miao, C. Babin, M. Widmann, M. Niethammer, J. Ul Hassan, N. Morioka, I. G. Ivanov, F. Kaiser, J. Wrachtrup, and D. D. Awschalom, Developing silicon carbide for quantum spintronics, Appl. Phys. Lett. **116**, 190501 (2020).

[7] S. Castelletto and A. Boretti, Silicon carbide color centers for quantum applications, J. Phys. Photonics **2**, 022001 (2020).

[8] W. F. Koehl, B. B. Buckley, F. J. Heremans, G. Calusine, and D. D. Awschalom, Room temperature coherent control of defect spin qubits in silicon carbide, Nature (London) **479**, 84 (2011).

[9] D. J. Christle, A. L. Falk, P. Andrich, P. V. Klimov, J. U. Hassan, N. T. Son, E. Janzén, T. Ohshima, and D. D. Awschalom, Isolated electron spins in silicon carbide with millisecond coherence times, Nat. Mater. **14**, 160 (2015).

[10] M. Widmann, S.-Y. Lee, T. Rendler, N. T. Son, H. Fedder, S. Paik, L.-P. Yang, N. Zhao, S. Yang, I. Booker, A. Denisenko, M. Jamali, S. A. Momenzadeh, I. Gerhardt, T. Ohshima, A. Gali, E. Janzén, and J. Wrachtrup, Coherent control of single spins in silicon carbide at room temperature, Nat. Mater. **14**, 164 (2015).

[11] A. Boretti, Q. Li, and S. Castelletto, Pioneering the future with silicon carbide integrated photonics, Opt. Laser Technol. **181**, 111910 (2025).

[12] N. T. Son, P. Carlsson, J. ul Hassan, E. Janzén, T. Umeda, J. Isoya, A. Gali, M. Bockstedte, N. Morishita, T. Ohshima, and H. Itoh, Divacancy in 4H-SiC, Phys. Rev. Lett. **96**, 055501 (2006).

[13] A. Falk, B. B. Buckley, G. Calusine, W. F. Koehl, V. V. Dobrovitski, A. Politi, C. A. Zorman, P. X.-L. Feng, and D. D. Awschalom, Polytype control of spin qubits in silicon carbide, Nat. Commun. **4**, 1819 (2013).

[14] N. T. Son, D. Shafizadeh, T. Ohshima, and I. G. Ivanov, Modified divacancies in 4H-SiC, J. Appl. Phys. **132**, 025703 (2022).

[15] Q. Li, J.-F. Wang, F.-F. Yan, J.-Y. Zhou, H.-F. Wang, H. Liu, L.-P. Guo, X. Zhou, A. Gali, Z.-H. Liu, Z.-Q. Wang, K. Sun, G.-P. Guo, J.-S. Tang, H. Li, L.-X. You, J.-S. Xu, C.-F. Li, and G.-C. Guo, Room-temperature coherent manipulation of single-spin qubits in silicon carbide with a high readout contrast, Nat. Sci. Rev. **9**, nwab122 (2022).

[16] V. Ivády, J. Davidsson, N. Delegan, A. L. Falk, P. V. Klimov, S. J. Whiteley, S. O. Hruszkewycz, M. V. Holt, F. J. Heremans, N. T. Son, D. D. Awschalom, I. A. Abrikosov, and A. Gali, Stabilization of point-defect spin qubits by quantum wells, Nat. Commun. **10**, 5607 (2019).

[17] B. Magnusson, N. T. Son, A. Csore, A. Gällström, T. Ohshima, A. Gali, and I. G. Ivanov, Excitation properties of the divacancy in SiC, Phys. Rev. B **98**, 195202 (2018).

[18] G. Wolfowicz, C. P. Anderson, A. L. Yeats, S. J. Whiteley, J. Niklas, O. G. Poluektov, F. J. Heremans, and D. D. Awschalom, Optical charge state control of spin defects in 4H-SiC, Nat. Commun. **8**, 1876 (2017).

[19] D. A. Golter and C. W. Lai, Optical switching of defect charge states in 4H-SiC, Sci. Rep. **7**, 13406 (2017).

[20] D. Shafizadeh, J. Davidsson, T. Ohshima, I. A. Abrikosov, N. T. Son, and I. G. Ivanov, Selection rules in the excitation of the divacancy and the nitrogen-vacancy pair in 4H- and 6H-SiC, Phys. Rev. B **109**, 235203 (2024).

[21] N. T. Son, X. T. Trinh, L. S. Løvlie, B. G. Svensson, K. Kawahara, J. Suda, T. Kimoto, T. Umeda, J. Isoya, T. Makino, T. Ohshima, and E. Janzén, Negative-U system of carbon vacancy in 4H-SiC, Phys. Rev. Lett. **109**, 187603 (2012).

[22] See Supplemental Material at http://link.aps.org/supplemental/10.1103/PhysRevB.111.165201 for further details on the experimental geometry, validity of the excitation selection rules at elevated temperatures, and experimental data supporting the photoluminescence upconversion mechanism.

[23] F.-F. Yan, J.-F. Wang, Q. Li, Z.-D. Cheng, J.-M. Cui, W.-Z. Liu, J.-S. Xu, C.-F. Li, and G.-C. Guo, Coherent control of defect spins in silicon carbide above 550 K, Phys. Rev. Appl. **10**, 044042 (2018).

[24] J.-F. Wang, F.-F. Yan, Q. Li, Zh.-H. Liu, J.-M. Cui, Z.-D. Liu, A. Gali, J.-S. Xu, Ch.-F. Li, and G.-C. Guo, Robust coherent control of solid-state spin qubits using anti-Stokes excitation, Nat. Commun. **12**, 3223 (2021).

[25] Wu-Xi Lin, J.-F. Wang, Q. Li, J.-Y. Zhou, Z.-X. He, Z.-H. Hao, H. Li, L.-X. You, J.-S. Xu, C.-F. Li, and G.-C. Guo, Room temperature coherent control of a single solid-state spin under anti-Stokes excitation, Phys. Rev. B **108**, 235312 (2023).